Original Article

http://dx.doi.org/10.3348/kjr.2012.13.2.152
pISSN 1229-6929 · eISSN 2005-8330
Korean J Radiol 2012;13(2):152-164

Korean Journal of Radiology
KJR

80-kVp CT Using Iterative Reconstruction in Image Space Algorithm for the Detection of Hypervascular Hepatocellular Carcinoma: Phantom and Initial Clinical Experience

Saebeom Hur, MD, Jeong Min Lee, MD, PhD, Soo Jin Kim, MD, PhD, Ji Hoon Park, MD, Joon Koo Han, MD, PhD, Byung Ihn Choi, MD, PhD

All authors: Department of Radiology, Seoul National University Hospital, Seoul National University College of Medicine, Seoul 110-744, Korea

Objective: To investigate whether the low-tube-voltage (80-kVp), intermediate-tube-current (340-mAs) MDCT using the Iterative Reconstruction in Image Space (IRIS) algorithm improves lesion-to-liver contrast at reduced radiation dosage while maintaining acceptable image noise in the detection of hepatocellular carcinomas (HCC) in thin (mean body mass index, 24 ± 0.4 kg/m^2) adults.

Subjects and Methods: A phantom simulating the liver with HCC was scanned at 50-400 mAs for 80, 100, 120 and 140-kVp. In addition, fifty patients with HCC who underwent multiphasic liver CT using dual-energy (80-kVp and 140-kVp) arterial scans were enrolled. Virtual 120-kVP scans (protocol A) and 80-kVp scans (protocol B) of the late arterial phase were reconstructed with filtered back-projection (FBP), while corresponding 80-kVp scans were reconstructed with IRIS (protocol C). Contrast-to-noise ratio (CNR) of HCCs and abdominal organs were assessed quantitatively, whereas lesion conspicuity, image noise, and overall image quality were assessed qualitatively.

Results: IRIS effectively reduced image noise, and yielded 29% higher CNR than the FBP at equivalent tube voltage and current in the phantom study. In the quantitative patient study, protocol C helped improve CNR by 51% and 172% than protocols A and B ($p < 0.001$), respectively, at equivalent radiation dosage. In the qualitative study, protocol C acquired the highest score for lesion conspicuity albeit with an inferior score to protocol A for overall image quality ($p < 0.001$). Mean effective dose was 2.63-mSv with protocol A and 1.12-mSv with protocols B and C.

Conclusion: CT using the low-tube-voltage, intermediate-tube-current and IRIS help improve lesion-to-liver CNR of HCC in thin adults during the arterial phase at a lower radiation dose when compared with the standard technique using 120-kVp and FBP.

Index terms: *Hepatocellular carcinoma; Low tube voltage; Iterative reconstruction; 80-kVp; Computed tomography; Image quality*

INTRODUCTION

Hepatocellular carcinoma (HCC) is the most common primary malignant hepatic tumor worldwide, and its early detection is paramount to a successful treatment. Several previous studies have demonstrated that HCCs in their

Received August 23, 2011; accepted after revision October 14, 2011.
This study was supported by a grant from the National R&D Program for Cancer Control, Ministry for Health and Welfare, Republic of Korea (1120310).
The abstract of this work was presented at RSNA 2010, in Chicago, USA.
Corresponding author: Jeong Min Lee, MD, Department of Radiology, Seoul National University Hospital, Seoul National University College of Medicine, 101 Daehak-ro, Jongno-gu, Seoul 110-744, Korea.
• Tel: (822) 2072-2584 • Fax: (822) 743-6385 • E-mail: jmsh@snu.ac.kr

Korean Journal of Radiology
KJR

early stage showed significantly better survival rates than those in their advanced stage (1, 2). An important factor in the diagnosis of HCCs on dynamic computed tomography (CT) is the lesion-to-liver contrast (1-3) which is directly related to the intense enhancement of a lesion in the late arterial phase (4-6). However, accurate diagnosis of small HCC nodules in a cirrhotic liver on CT can be challenging as some HCCs show only a subtle increase in hepatic arterial blood supply (7-9). In addition, despite the tremendous contributions of CT to health care for patients with liver cirrhosis and HCC, some attention must also be given to the risk associated with the ionizing radiation received during the frequent use of CT for the diagnosis and treatment monitoring of HCCs (10-12). Thus, there is currently a clinical demand to reduce radiation dosage in addition to increasing the sensitivity of CT to reveal small attenuation increments of HCC nodules.

Many investigators have shown that a low tube voltage (80 kVp) CT scan can provide a better lesion-to-liver contrast for hypervascular focal liver lesions when compared with a 120 or 140 kVp CT scan in patients with small to medium body habitus (6, 13-19). This can be explained by the higher attenuation of X-ray beams caused by the closer energy level of a low tube voltage to the K edge of iodine (17, 18). The resulting lower radiation dose, which is proportional to the square of the tube voltage, is an added benefit to the low tube voltage CT scan (10, 16). Indeed, reducing the tube voltage from 120 to 80 kVp has been reported to lead to a 65% decrease in radiation dose at a constant tube current (20). However, the main drawback of the low tube voltage technique is that the reduced photon flux due to the higher absorption of low-energy photon which creates a greater image noise (10). Therefore, to realize an overall improvement of contrast-to-noise ratio (CNR) for hypervascular liver lesions at low tube voltage, image noise has to be diminished effectively (4, 21).

Several approaches have been attempted in order to decrease the noise at low tube-voltage. One is to raise the tube current-time product (4, 6, 15). However, the increase of tube current is limited by the heat characteristics of the rotating anode, while the increase in X-ray exposure duration is limited by the gantry rotation time in order to be less impacted by motion artifacts. Another method is to exploit post-processing development such as an iterative reconstruction process through adaptive statistical iterative reconstruction (ASIR) or Iterative Reconstruction in Image Space (IRIS) algorithm, which can lower the image noise using calculation and correction in a repeated circuit (22-24). A previous study by Marin et al (15) demonstrated that CT scanning using a low tube voltage, high-tube-current (675 mAs) and the ASIR algorithm increased the CNR of aorta, liver, and pancreas by a factor of 1.3 to 2.4 when compared with those with either 140 kVp or 80 kVp and conventional filtered back-projection (FBP) reconstruction. However, the study population in their study consisted of only 10 patients and the contrast of HCC was not evaluated.

In this study, we attempted to investigate whether an low tube voltage (80 kVp), intermediate tube current (340 mAs) CT using the IRIS algorithm improves lesion-to-liver CNR at a lower radiation dose in patients with HCC while maintaining an acceptable level of image noise compared with a standard 120 kVp CT scan using FBP reconstruction.

MATERIALS AND METHODS

Phantom Study

Phantom Preparation

A liver phantom was created using agar mixed with a water-soluble contrast agent (Diatrizoatemeglumine and diatrizoate sodium-solution; Gastrografin, Bayer-Schering, Berlin, Germany) to attain a similar attenuation coefficient of the liver parenchyma during the late arterial phase (Fig. 1). From the liver CT images of our pilot study using the dual-energy CT scanning mode for HCCs, we were able to measure

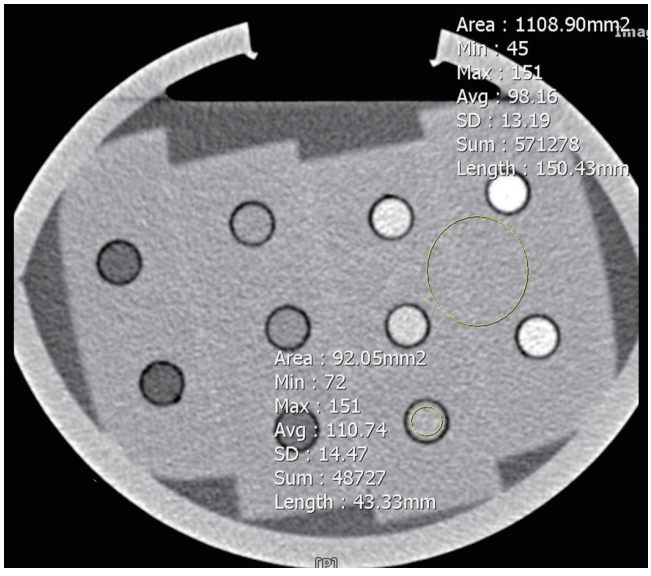

Fig. 1. Axial CT image of phantom at tube voltage of 100 kVP and 150 mAs. Fifth tube was selected as target lesion to simulate subtle hypervascular HCC nodules.

the attenuation value of the liver during the late arterial phase as 64 ± 7.8 HU at 120 kVp (0.3 linear blending image). Based on this data, the amount of Gastrografin (0.8 mL per 100 mL agar) was selected to simulate a contrast-enhanced liver during the late arterial phase. The mean attenuation values of the liver phantom were 78 HU for 120 kVp scanning and 130 HU for 80 kVp scanning.

Ten conical 15-mL tubes (Falcon; BD Biosciences, Franklin Lakes, NJ, USA) were filled with various concentrations of iodinated contrast medium (25). These tubes were placed in the central portion of the liver phantom to simulate HCC nodules in the liver. The consequent liver and HCC phantom was placed in a water-filled plastic container which was cylindrical with elliptical cross sections. The phantom was shaken just before each CT scan to minimize the risk of iodine sediment in the tubes. The mean attenuation values were 14, 18, 53, 70, 87, 117, 133, and 139 HU for 120 kVp. The 5th tube was selected as the target lesion to simulate subtle hypervascular HCC nodules in the late arterial phase with a lesion-to-liver attenuation difference of 10 HU at 120 kVp.

Scan Protocol

We used the larger tube of the dual source CT scanner (SOMATOM Definition; Siemens, Forchheim, Germany) in the single energy mode (collimation, 14 x 1.2 mm; rotation time, 1 second; pitch, 0.85; peak kVp 80, 100, 120, and 140). A total of 10 scans were performed with 50, 75, 100, 125, 150, 200, 250, 300, 350 and 400 mAs for each kVp.

CT Image Reconstruction

Reconstruction of raw CT data was performed using standard FBP and IRIS algorithms, which are embedded in the CT scanners, respectively (Somatom Definition; Siemens). IRIS is an iterative reconstruction technique in which the signal generation process is modeled and a correction loop is introduced into the image reconstruction (26, 27). Several image processing steps including reprojection, regularization, and a chain of iterative non-linear image processing steps are required for IRIS reconstruction. Once an image has been reconstructed from the measured projections, ray tracing is performed to calculate new projections that exactly represent the reconstructed image. This step, called reprojection, simulates the CT measurement process, but with the image as the "measurement object." The deviation between the measured and the calculated projections is used to derive correction projections, and then to reconstruct a correction image and update the original image. This loop is continued until the deviation between the measured and the calculated projections is smaller than a predefined limit (27). Each time the original image is updated, a non-linear image processing algorithm is used to enhance spatial resolution at higher object contrasts and to reduce image noise in low contrast areas. This step is called "regularization", and it is essential for the noise reduction of iterative reconstruction. The next step involves a chain of iterative non-linear image processing steps, which are locally adapted and optimized according to the local image noise and image structure (26, 27).

Data Analysis and Statistical Methods

All measurements were performed at a commercially available workstation (XW6200; Hewlett-Packard, CA, USA) with the PACS software (Maroview 5.4; Infinitt, Seoul, Korea). Regions of interest (ROI) were selected for the simulated lesion and agar background of the phantom. The contrast-to-noise-ratio (CNR) of the lesion was calculated as $CNR = (ROI_{Lesion}\text{-}ROI_{Background}) / \sigma$, where ROI_{Lesion} and represents the mean attenuation value of the simulated lesion. Further, $ROI_{Background}$ is the mean attenuation value of the phantom background, and σ is the standard deviation of the phantom background attenuation value. The constant sizes of the maintained ROI were approximately 1100 mm^2 for the background and 92.05 mm^2 for the simulated lesion. The image noise was determined by the standard deviation of the ROI placed on the agar portion simulating the liver parenchyma.

As for a given beam quality, the CNR increases in proportion to the square root of the radiation dose; thus, direct comparisons of image quality characteristics between images with different radiation dose was impossible. To solve this problem, the CNR was normalized to an effective dose (ED) for each protocol by using a figure of merit (FOM), which was defined as follows: $FOM = CNR^2 / ED$. The FOM enabled the assessment of CNR independent of the tube current and effective dose (4, 28, 29).

Computed tomography dose index (CTDIvol) autocalculated by an implemented program, was used as the effective dose. As we used only one phantom and CTDIvol was not a dependent value of the scan length, using CTDIvol as the effective dose seemed optimal (29, 30).

Korean Journal of Radiology
KJR

Patient Study

Patients

We obtained approval for this retrospective study from the institutional review board of our hospital. Written informed consent was not required because the image data were obtained from routine liver CT examinations retrospectively. The case accrual process (Fig. 2) and the control of data and information were managed by two authors (S.H. and J.M.L.).

From March through May of 2010, 117 consecutive patients with known or suspected HCC underwent multiphasic liver CT imaging with a 64-channel dual-energy multi-row detector CT scanner (Somatom Definition). The presence or suspicion of HCC was determined on the basis of the results of prior cross-sectional imaging examinations (n = 86), abnormally increased tumor marker (α-fetoprotein) levels (n = 20) or both (n = 11). We retrospectively reviewed the patient medical records and radiologic reports using our electronic medical records system (Bestcare; Ezcaretech, Seoul, Korea). Fifty patients (38 men and 12 women; mean age, 61 years,) were included in the study group after exclusion of 67 patients due to the following reasons: (a) Thirty-seven patients had innumerable disseminated HCC (more than 10 typical early-enhancing/delayed-washout nodules on dynamic CT). (b) Twenty-six patients were proven not to have HCCs according to the reference standard. (c) Four patients were lost to follow up before obtaining confirmation of liver nodules according to the reference standard.

The mean body mass index (body mass index = weight in kg divided by the square of height [m]) was 24 ± 0.4 kg/m^2 (ranging from 17.2 to 30.7 kg/m^2).

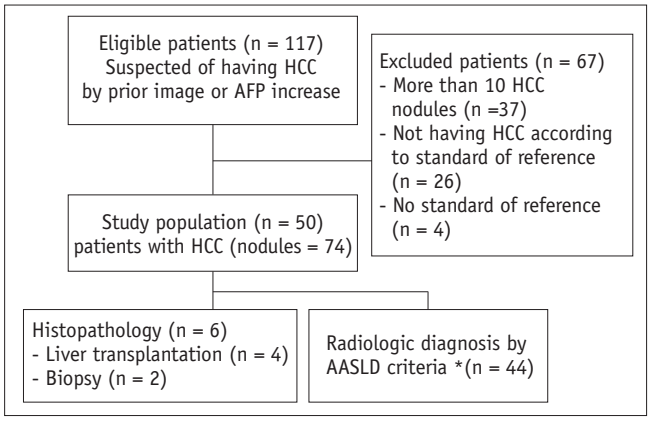

Fig. 2. Flow chart of study population enrollment based on recommended standards for reporting diagnostic accuracy and proof of tumor burden. *Follow-up was performed with multidetector CT, MR imaging, or both after minimum of 6 months. AASLD = American Association for Study of Liver Disease

Lesion Confirmation: Reference Standard

The overall lesion confirmation process summarized in Figure 2 was obtained in consensus by two radiologists (J.H.P and J.K.H, with 3 and 20 years of clinical experience, respectively) who had not participated in the CT interpretation sessions. In total, the 50 patients proved to have 74 HCC nodules. There were 32 patients with one lesion, 13 patients with two lesions, four patients with three lesions and one patient with four lesions. Overall, the mean transverse diameter of the nodules was 1.37 cm (range: 1.0-3.3 cm).

In four patients (4/50, 8%) who had undergone liver transplantation, the presence of all lesions identified radiographically was determined histologically on a per-lesion basis by means of thorough interpretation of the available preoperative images obtained at CT, MR, or intraoperative ultrasonography, as well as the surgical and pathologic findings. Gross and histologic analyses of all resected livers were performed by a hepatobiliary pathologist with 10 years of clinical experience. All resected livers were initially sectioned at no more than 5-mm intervals in the sagittal plane. In addition, two patients (2/50, 4%) had a histologic diagnosis of HCC through a liver biopsy and underwent radiofrequency ablation (RFA). Follow-up CT and/or MR imaging was performed at least 6 months after the procedure, and there was no evidence of HCC in the residual liver. The other 44 patients (44/50, 88%) were diagnosed radiologically as having HCCs according to the practice guidelines from the American Association for the Study of Liver Disease, which suggested the typical vascular pattern (hypervascular in the late arterial phase, and washes out in the portal/venous phase) in one dynamic imaging technique for hepatic nodules with a diameter larger than 1 cm as the diagnostic criteria in a cirrhotic liver (1). These patients were treated by either RFA or transcatheter arterial chemoembolization (TACE), and follow-up imaging studies were performed until at least 6 months after the initial diagnosis.

Scan Protocol

Multiphasic liver CT scans consisting of precontrast, late arterial, portal venous, and equilibrium phase images were routinely obtained using a dual energy CT scanner (SOMATOM Definition, Siemens). Only late arterial images

were obtained in the dual energy mode with each X-ray tube operating at 80 kVp and 140 kVp, respectively (29, 31). Precontrast, portal venous and equilibrium phase images were obtained using 120 kVp tube energy. Iodinated contrast media of 370 mgI/mL (iopromide, Ultravist 370; Bayer-Schering, Berlin, Germany) at a dose of 1.5 mL/kg (= 555 mgI/kg) per body weight, was injected for 30 seconds using a power injector (Stellant Dual; Medrad, Indianola, PA, USA) and was followed by injection of 30 to 40 mL of normal saline (32). Timing for the late arterial phase scan was determined using the care bolus technique (Siemens), i.e., late arterial phase scanning was automatically started 17 seconds after the attenuation coefficient of the abdominal aortic blood reached 80 HU at 140 kVp (32, 33). Late arterial phase images were obtained in the dual energy mode using the following parameters: collimation, 14 x 1.2 mm; rotation time, 0.5 second; pitch, 0.85. The automatic dose modulation protocol provided by the manufacturer (CareDose4D, Siemens), adjusted tube current in real-time to maintain image noise at the optimal level (34). The reference tube current time product was set at 80 mAs for a 140 kVp tube and at 340 mAs for a 80 kVp tube. The tube current required of a 80 kVp tube was roughly four times that of a 140 kVp tube in order to match the noise level to the possible extent (35). These tube currents were chosen so that the images created are approximately dose-matched compared with a single source CT acquisition at 120 kVp when the CTDIvol of both tubes were added. The reference tube currents were 150 mAs for precontrast and 210 mAs for portal venous and equilibrium phase scan settings. The effective dose for arterial liver scanning with dual energy was approximately 2.63 mSv. The mean dose ratio between 140 kVp tube and 80 kVp tube was 1.3 : 1. Thus, the effective dose for arterial liver scanning with a 80 kVp tube was approximately 1.12 mSv. The effective dose for precontrast scans using a 120 kVp tube with a reference current of 150 mAs was 1.11 mSV, whereas the sum of the effective dose for portal venous and equilibrium phase scanning using a 120 kVp tube with a reference current of 210 mAs was 6.73 mSv. Therefore, the total effective dose for our liver protocol CT scanning was approximately 10.47 mSv (29). The effective doses for these protocols were computed according to published guidelines (36).

CT Image Reconstruction

The virtual 120 kVp images of late arterial phase were generated by linearly blending the 140 kVp and 80 kVp raw image with a 0.3 weighting factor and reconstructed into image sets for protocol A by using the standard FBP algorithm with a soft-tissue kernel (D30s) (29). The 80 kVp raw data were reconstructed into protocol B image sets by using the standard FBP algorithm with a soft-tissue kernel (D30s) and into protocol C image sets using the IRIS algorithm with a soft tissue iterative kernel (I30s) (Siemens Medical Solutions) (Fig. 3). In our study, the average reconstruction time for the IRIS algorithm was approximately 5 images per second while that for the standard FBP reconstruction algorithm was approximately

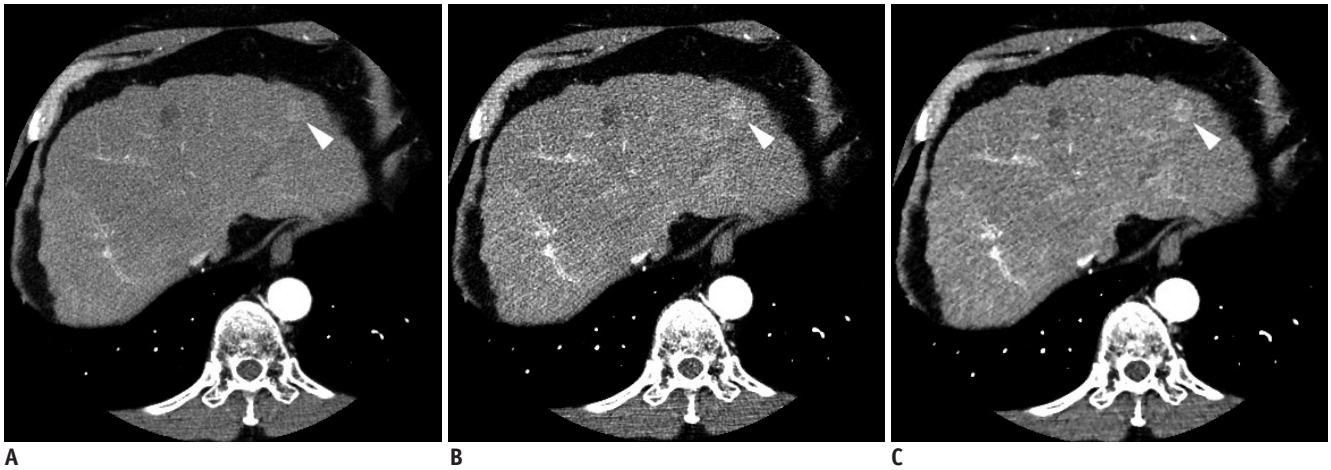

A B C

Fig. 3. Axial contrast-enhanced multidetector CT images obtained by using preset soft-tissue window (window width, 300 HU; window level, 40 HU) in 61-year-old man with HCC nodule in left lobe of liver. Images obtained during late arterial phase with **(A)** protocol A (linearly blended virtual 120 kVp, FBP), **(B)** protocol B (80 kVp, FBP), and **(C)** protocol C (80 kVp, IRIS) show substantially reduced image noise with protocol C compared to image noise with protocol B. Note reduced conspicuity of hypervascular liver tumors in due to decreased iodine attenuation at higher tube voltage settings compared with tumor conspicuity in B and C.

Korean Journal of Radiology
KJR

40 images per second.

Quantitative Study

An abdominal radiologist (S.H, with 3 years of experience in gastrointestinal and hepatobiliary imaging), aware of the location of confirmed HCC lesions, performed the quantitative measurements. The three image sets, obtained with protocols A, B, and C in each patient, were displayed side by side with a preset soft-tissue window (window width, 300 HU; window level, 40 HU). We measured the mean CT attenuation values (in Hounsfield units) in the HCC nodules, aorta, liver, pancreas and bilateral paraspinal muscles by manually placing circular ROIs (15). The attenuation of HCC nodules was recorded from a single drawn ROI (mean number of pixels, 80; range, 12-644 pixels) that was as large as the nodule at the image level, which showed the largest diameter of the lesion. Lipiodolized or necrotic portions which showed heterogeneous attenuation, if any, were carefully avoided (Fig. 4). The attenuation of the aorta was recorded from a single drawn ROI (mean number of pixels, 312; range, 154-2341 pixels) that was as large as the vessel lumen. Calcifications and/or soft plaques of the aortic wall were carefully avoided. The attenuation of the liver was recorded as the mean measurement of four ROIs (mean number of pixels, 524; range, 109-1711 pixels) placed in the right anterior, right posterior, left medial and left lateral segments of the liver. Areas of focal changes in parenchymal attenuation, large vessels, and prominent artifacts, if any, were carefully avoided. The attenuation of the pancreas was recorded as the mean measurement of three ROIs (mean number of pixels, 113; range, 22-379 pixels), which were placed at the level of the pancreatic head, body, and tail. Areas of focal changes in parenchymal density, large vessels, pancreatic ducts, and prominent artifacts were carefully avoided. The attenuation of the two paraspinal muscles was recorded from two ROIs (mean number of pixels, 497; range, 171-950 pixels) while excluding macroscopic areas of fat infiltration. For each protocol, image noise was measured as the standard deviation of the pixel values from a circular ROI (mean number of pixels, 247; range, 30-924 pixels) drawn in a homogeneous region of the subcutaneous fat of the anterior abdominal wall. For all measurements, the size, shape, and position of the ROIs were kept constant among the three protocols by applying a copy and paste function at the workstation.

For each of the three protocols, CNR of the lesion was calculated using the following equation: $CNR = (ROI_{Lesion} - ROI_{Liver}) / \sigma$, where ROI_{Lesion} is the attenuation of the HCC nodule, ROI_{Liver} is the mean attenuation for the liver parenchyma, and σ is the mean image noise. Similarly, CNR relative to muscle for the aorta, liver, and pancreas was calculated by the following equation: $CNR = (ROI_{Organ} - ROI_{Muscle}) / \sigma$, where the ROI_{Organ} is the mean attenuation of the organ at interest, and the ROIMuscle is the mean attenuation of the paraspinal muscles (15).

As in the phantom study, CNR values for lesions or organs of each protocol were normalized to the effective dose by using an FOM (Fig. 5) (4, 28, 29). To establish a similar

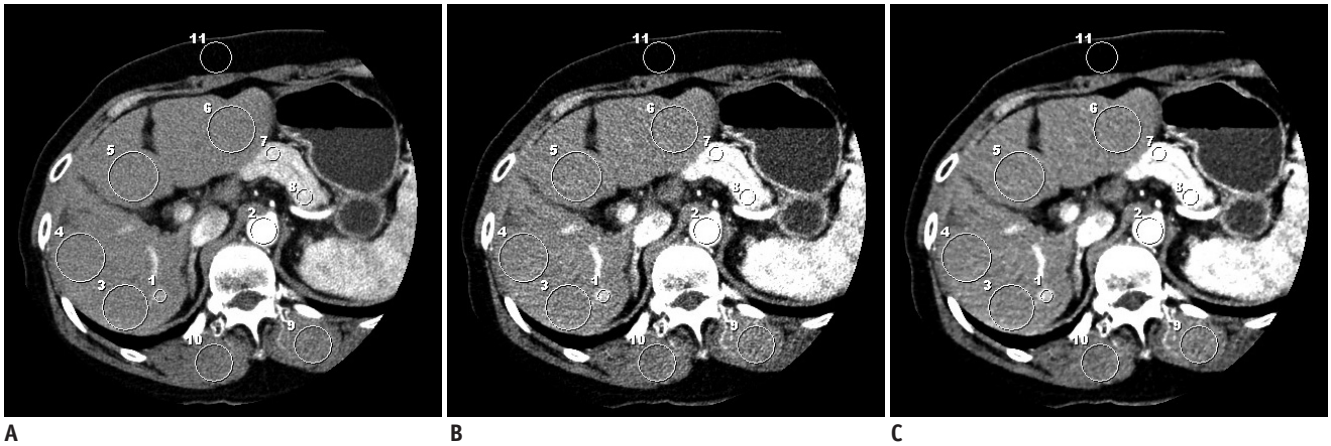

Fig. 4. Axial contrast-enhanced multidetector CT images obtained in 45-year-old man during late arterial phase with (A) protocol A (linearly blended virtual 120 kVp, FBP), (B) protocol B (80 kVp, FBP), and (C) protocol C (80 kVp, IRIS), which show ROIs manually drawn on HCC nodule (ROI 1), aorta (ROI 2), liver (ROIs 3-6), pancreas (ROIs 7, 8), paraspinal muscle (ROI 9, 10), and subcutaneous fat of anterior abdominal wall (ROI 11). Another ROI was drawn in other axial image (not shown) to measure attenuation value of pancreatic head. For all measurements, size, shape, and position of ROIs were kept constant among three protocols by applying copy-and-paste function at workstation.

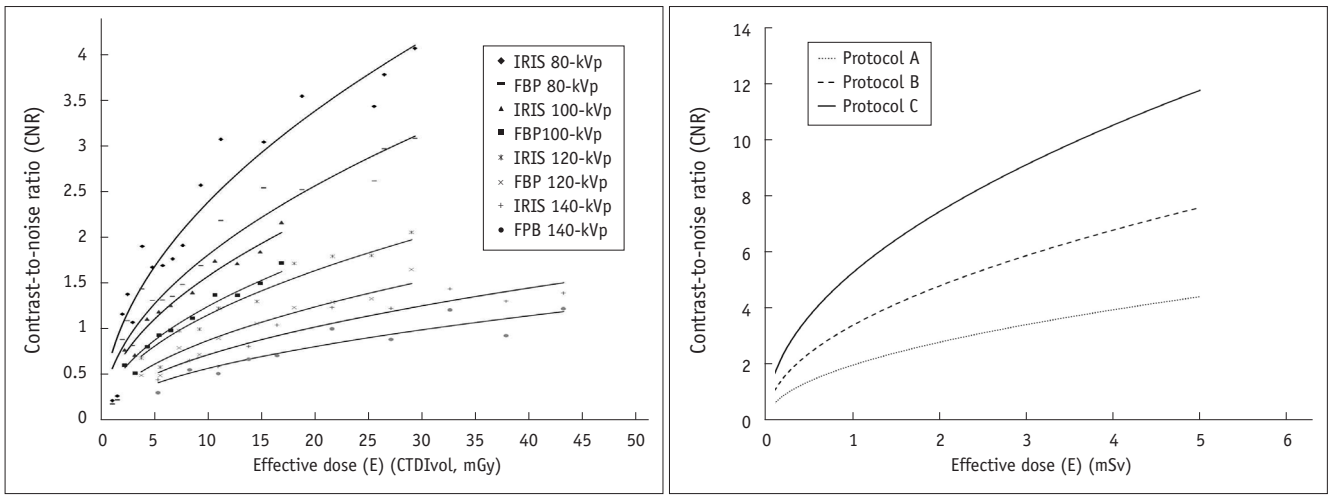

A B

Fig. 5. Relationship of CNR versus effective dose.
(A) Scatterplots and non-linear regression of lesion-to-background CNR versus effective dose at each kVp and reconstruction method in phantom study. The non-linear regression fit is represented by following equation, CNR = √(FOM x ED). Regression analysis resulted in FOM values from 0.03 to 0.58 for each condition with *p* values of less than 0.001. **(B)** Imaginary graphs of lesion-to-liver CNR versus effective dose for three CT protocols in patient study by following equation of CNR = √FOM x ED, which were proven in phantom study. Lesion-to-liver CNR can be increased in protocol C moreso than in protocols A or B at constant effective dose. Alternatively, effective dose can be reduced in protocol C moreso than in protocols A or B.

independent relationship for image noise, an FOM for the image noise (FOMN) normalized to the dose was also calculated using the following formula: FOMN = 1 / (σ^2 · ED), where σ^2 is the squared noise value (15).

Qualitative Study

Two radiologists (S.J.K and J.M.L, with 10 and 20 years of post-training experience, respectively, in interpreting abdominal CT) independently reviewed the late arterial phase CT images. To minimize recall bias, an image set from the three protocols of each patient was randomly allocated to three separate reading sessions with an interval of two weeks; in this manner, an image set of a patient appeared only once during each reading session. The radiologists evaluated HCC lesion conspicuity, image noise, and overall image quality, and were blinded to the CT parameters and reconstruction methods. However, information on the number and location of confirmed HCC lesions according to the reference standard were provided in order to allow a decision on lesion conspicuity. During the review, the observers were allowed to alternate only between a soft-tissue window (width, 300 HU; level, 40 HU) and a dedicated liver window (width, 150 HU; level, 90 HU).

The criteria for image grading were consensually established between the readers prior to the start of image reading. HCC lesion conspicuity was assessed on a five-point scale; score 5, definitely distinct; score 4, fairly distinct; score 3, moderately distinct; score 2, barely distinct; and score 1, not distinct (14). HCC lesion conspicuity was recorded as "definitely distinct" when the HCC lesion had a higher attenuation than the intrahepatic portal vein and a well-defined margin from the peripheral hepatic parenchyma. It was considered "fairly distinct" when an HCC had higher attenuation than the intrahepatic portal vein but had an ill-defined margin or similar attenuation with the portal vein and well-defined margin. It was considered "moderately distinct" when an HCC had similar attenuation compared to the portal vein and ill-defined margin. It was considered "barely distinct" when an HCC had a lower attenuation value than the portal vein but was relatively distinguishable from peripheral hepatic parenchyma. It was considered "not distinct" when the lesion could not be distinguished from the peripheral hepatic parenchyma without any provided information regarding the location of the lesion. For analysis of image noise and overall image quality, a three-point ordinal scale was used as follows: score 3, excellent; score 2, acceptable; and score 1, unacceptable (17). A rating of "excellent" for image noise was assigned when mottling was minimal or less than appreciable levels. The image noise was considered to be "acceptable" in cases with an average amount of mottle or graininess, satisfactory visualization of small anatomic structures such as blood vessels, and variable attenuation of the interface between structures. Image

Korean Journal of Radiology
KJR

noise was considered to be "unacceptable" in cases where the amount of mottle interfered with the visualization of these structures. Overall image quality was graded according to the observers' subjective impression of the image. Image noise was considered to be "excellent" when the impression of the image quality was equivalent or superior to the standard liver CT technique in current clinical practice. Image noise was considered to be "acceptable" when the impression of the image quality was slightly inferior to the current standard but still adequate for HCC lesion detection. Image noise was considered to be "unacceptable" when the impression of the image quality was so poor that it was not adequate for lesion detection. All image reviews were performed on PACS software (Maroview 5.4, Infinitt) running on a workstation (XW6200, Hewlet-Packard), with two 2048 × 1536-pixel 20.8-inch monochrome liquid crystal display monitors (ME315L; Totoku Electric, Tokyo, Japan).

Statistical Analysis

For the evaluation of differences in image noise, CNR, and corresponding FOM among the three protocols, a repeated-measures analysis of variance (RMANOVA) was performed, with protocols serving as the analysis of variance factors. The estimates from this model were compared in pairwise fashion using the Bonferroni adjustment for the three comparisons. For data which could not pass the Kolmogorov-Smirnov normality test, the nonparametric Friedman test was applied instead of the RMANOVA (29). The Friedman test was used to investigate statistically significant differences in qualitative scores recorded by the two radiologists. If there was a statistically significant difference among the groups, pairwise comparisons were performed using the Steel-Dwass test. For all studies, a difference with a p value of less than 0.05 was considered to be statistically significant. Interobserver agreement was evaluated using kappa statistics (37). The scale for the k coefficients for interobserver agreement was as follows: less than 0.20, poor; 0.21-0.40, fair; 0.41-0.60, moderate; 0.61-0.80, substantial; and 0.81-1.00, almost perfect. Statistical analysis software (SPSS for Windows, version 17.0, SPSS, Chicago, IL; SigmaPlot 11.0, Systat Software, San Jose, CA, USA) was used for all statistical analyses in our study.

Table 1. Result of Calculated FOM* in Phantom Study

Tube-voltage (kVp)	FBP	IRIS
80	0.33	0.58
100	0.16	0.24
120	0.08	0.14
140	0.03	0.05

Note.— *FOM = CNR^2 / ED. FOM = figure of merit, CNR = contrast-to-noise ratio, ED = effective dose

RESULTS

Phantom Study

Scatterplots of lesion-to-background CNR versus effective dose for each kVp and reconstruction methods can be seen in Figure 5. The non-linear regression fit was represented by the following equation, CNR = √(FOM x ED), which was deduced by the definition of FOM (FOM = CNR^2 / ED). FOM values were summarized by this regression analysis in Table 1. The FOM increased as the tube voltage decreased from 140 to 80 kVp. The FOM of the images reconstructed with IRIS was higher than that with FBP by an average 65.5% at each tube voltage (75.7% at 80 kVp, 53.0% at 100 kVp, 74.1% at 120 kVp, and 59.5% at 140 kVp, respectively), which means IRIS achieved a 28.6% higher CNR than conventional FBP at an equivalent effective dose.

Patient Study

Quantitative Study

Mean image noise was significantly lower with protocol A (13.5 HU) and protocol C (13.6 HU) than with protocol B (20.0 HU) (p = 0.001, both). There was no significant difference in image noise between protocol A and protocol C (p = 1.000). With the recognition that different radiation doses were delivered with each protocol, our FOM results indicated that the use of protocol C led to a nearly two-fold decrease in noise compared with the noise at protocols A and B (p < 0.001, both). In addition, protocol C achieved significantly higher lesion-to-liver CNR and lesion-to-liver FOM when compared with protocols A and B (p < 0.001, both) (Table 2). The ratio of lesion-to-liver FOM of protocol C to that of protocol A and to that of protocol B were 7.11 and 2.40, respectively. These are compatible with those of the phantom study, in which the ratio of FOM of 80 kVp image with IRIS (corresponding to protocol C) to that of 120 kVp image with FBP (corresponding to protocol A) and to that of 80 kVp image with FBP (corresponding to protocol B) were 7.36 and 1.71, respectively. Similarly, protocol C yielded significantly increased CNR and FOM values for the aorta, liver and pancreas when compared with protocols A and B with statistical significance (p < 0.001,

Table 2. Image Noise, CNR, FOM, and Effective Dose for Protocols A, B and C in Quantitative Patient Study

CT Parameter	Protocol A	Protocol B	Protocol C	*P* Value		
				Protocol C vs. Protocol A	Protocol C vs. Protocol B	Protocol A vs. Protocol B
Image noise (HU)	13.50 ± 0.30 (11.0-20.4)	20.0 ± 0.40 (14.9-27.1)	13.60 ± 0.40 (8.1-20.8)	1.000	0.001	0.001
CNR						
Lesion-to-liver	2.53 ± 0.17 (1.41-3.49)	2.84 ± 0.18 (1.77-3.65)	4.28 ± 0.29 (2.57-5.59)	0.001	0.001	0.041
Aorta	18.87 ± 0.55 (16.61-20.54)	20.39 ± 0.57 (18.49-23.00)	30.78 ± 1.00 (27.01-34.50)	0.001	0.001	0.008
Liver	0.96 ± 0.11 (0.53-1.3)	0.89 ± 0.090 (0.56-1.21)	1.32 ± 0.14 (0.79-1.75)	0.001	0.001	0.245
Pancreas	4.39 ± 0.16 (3.70-5.20)	3.76 ± 0.12 (3.26-4.31)	5.76 ± 0.20 (4.82-6.66)	0.001	0.001	0.001
FOM						
Lesion	3.88 ± 0.55 (0.87-5.28)	11.49 ± 1.90 (3.00-12.70)	27.58 ± 5.46 (6.28-30.45)	0.001	0.001	0.122
Aorta	149.59 ± 9.60 (120.6-172.4)	411.22 ± 27.09 (278.01-493.5)	961.24 ± 77.78 (601.5-1141.8)	0.001	0.001	0.001
Liver	0.61 ± 0.11 (0.096-0.69)	1.16 ± 0.22 (0.27-1.35)	2.58 ± 0.48 (0.59-3.07)	0.001	0.001	0.138
Pancreas	8.19 ± 0.61 (5.78-10.58)	14.02 ± 0.99 (9.61-16.91)	33.24 ± 2.58 (20.70-40.90)	0.001	0.001	0.002
Effect dose (mSv)	2.63 ± 0.09 (1.50-5.69)	1.12 ± 0.04 (0.65-2.46)	1.12 ± 0.04 (0.65-2.46)	0.001	-	0.001

Note.— Data are mean values ± standard errors of mean; numbers in parentheses represent ranges (25-75%).

all).

If the effective dose was kept constant with that of protocol A (mean 2.63 mSv), protocol C could yield significantly greater CNRs for the HCC nodule, aorta, liver and pancreas by factors of 2.72, 2.51, 2.73 and 2.04, respectively when compared with protocol A ($p < 0.001$ all) (Fig. 5). In addition, when protocol C was compared with protocol B, a similar finding of the increased CNRs in the HCC nodule, aorta, liver and pancreas (1.51, 1.50, 1.50 and 1.53 respectively) was observed with statistical significance ($p < 0.001$, all). Alternatively, when the CNR was kept constant, protocol C yielded on average an 83% decrease in effective dose compared with protocol A and a 54% decrease in effective dose compared with protocol B ($p < 0.001$, all).

Qualitative Study

The quality scores assigned by the two radiologists and the level of interobserver agreement are shown in Table 3. Both readers graded the highest score of lesion conspicuity for protocol C and a similar score of image noise between protocols A and C, while marking the lowest score for protocol B. Meanwhile, the score for overall image quality was higher in protocol A than in protocols B and C. Interobserver agreements on lesion conspicuity, image noise and overall image quality were moderate (Cohen's kappa = 0.47, 0.59 and 0.40, respectively).

DISCUSSION

In our study, low tube voltage (80 kVp), intermediate tube current (340 mAs) CT images using the IRIS algorithm during the late arterial phase showed better lesion conspicuity for hypervascular HCCs at a lower radiation dosage than standard 120 kVp CT images using the FBP algorithm, both quantitatively and qualitatively ($p < 0.05$). We believe that this could be attributed to the combined effect of increased contrast enhancement of the tumors compared with the surrounding liver tissue generated by the low tube voltage (80 kVp), as well as compensated image

Korean Journal of Radiology
KJR

Table 3. Qualitative Study Scores for CT Protocol A, B, and C

	Observer A			Observer B			Cohen's Kappa*
	A	B	C	A	B	C	
Lesion conspicuity	2.96	3.63	4.34	2.72	3.52	3.83	0.47
P value	< 0.05† A vs. B	< 0.05† B vs. C	< 0.05† C vs. A	< 0.05† A vs. B	> 0.05 B vs. C	< 0.05† C vs. A	
Image Noise	2.73	2.10	2.91	2.87	2.12	2.73	0.59
P value	< 0.05† A vs. B	< 0.05† B vs. C	> 0.05 C vs. A	< 0.05† A vs. B	< 0.05† B vs. C	> 0.05 C vs. A	
Overall Image Quality	2.86	2.20	2.20	2.88	2.53	2.33	0.40
P value	< 0.05† A vs. B	> 0.05 B vs. C	< 0.05† C vs. A	< 0.05† A vs. B	> 0.05 B vs. C	< 0.05† C vs. A	

Note.— Lesion conspicuity were rated on five-point scale, where 5, definitely distinct; 4, fairly distinct; 3, moderately distinct; 2, barely distinct; and 1, not distinct. Image noise and overall image quality were rated on three-point scale, where 3 was excellent; 2, acceptable; and 1, unacceptable. Data are mean scores. *Values were reported as follows: poor, less than 0.20; fair, 0.21–0.40; moderate, 0.41–0.60; substantial, 0.61–0.80; and almost perfect, 0.81–1.00, †Value shows statistically significant difference in pairwise comparison using Steel-Dwass test.

noise of the 80 kVp data set through the IRIS algorithm. The attenuation difference between a hypervascular HCC and the background liver parenchyma was increased as the tube voltage decreased from 120 to 80 kVp because of the increased attenuation of iodine at 80 kVp (4). However, this increased attenuation difference of the low tube voltage image with FBP reconstruction (protocol B) was offset by increased image noise, which is the most notable disadvantage of low tube voltage CT (13, 38, 39), and therefore, the lesion-to-liver CNR was similar to that of conventional CT imaging using the FBP reconstruction algorithm (protocol A). On the contrary, the increased attenuation difference of low tube voltage images with IRIS reconstruction (protocol C) resulted in higher CNR than protocol A by achieving similar image noise with protocol A. In addition, protocol C acquired the highest score for lesion conspicuity and an equivalent score with protocol A for image noise in the qualitative study. Based on our results, we believe that a late arterial phase CT scan at a low tube voltage and intermediate tube current setting using the IRIS algorithm may provide better conspicuity of small and/or subtly enhancing HCCs than standard 120 kVp imaging.

In our study which included many thin adults, an intermediate tube current was used for 80 kVp scanning with the IRIS algorithm, which resulted in a 41-84% decrease in the effective dose compared with 120 kVp scanning using the FBP algorithm, when the CNR was kept constant. Therefore, we believe that low tube voltage scanning with an intermediate tube current and the IRIS algorithm may result in a larger dose reduction than that of a higher tube current, and may be particularly beneficial for young patients with chronic liver disease or those with a previously treated HCC who are at high risk for hepatic neoplasms and need repeated multiphasic contrast-enhanced liver CT examinations during their life span. Our study results are in good agreement with the results of the previous study by Marin et al. (15), which demonstrated that the ASIR algorithm improves image quality compared with standard FBP reconstruction and has the potential to decrease radiation dose at low tube voltage, high-tube-current multidetector abdominal CT during the late hepatic arterial phase. However, there was a difference between the two studies: the intermediate tube current (approximately 340 mAs) was used for 80 kVp scanning in our study whereas high tube current (540 mAs) was used in the previous study (15). Had we selected a higher tube-current to offset the higher image noise, further reduction in image noise could have been possible at the cost of an increase in radiation dose. However, the application of higher tube current (> 600 mAs) can be limited by the type of CT scanner or vendor: the maximum tube current for the Definition scanner which was used in our study, was only 500 mAs. An additional difference between the two studies was that we analyzed the lesion to liver CNR of hypervascular HCCs in our study but only evaluated organ to muscle CNR was evaluated in the previous study. In addition, there were many patients with relatively small to medium body habitus with BMI smaller than 30 in our study, whereas there were patients with BMI higher than 30 in the previous study. Therefore, our study

results successfully demonstrated the advantage of low tube voltage and intermediate tube current CT imaging using the IRIS algorithm for the detection of HCC in thin adults. Moreover, we analyzed image sets with IRIS or FBP reconstruction using either standard tube-voltage or low tube voltage regarding lesion conspicuity, image noise and overall image quality qualitatively; however, a qualitative analysis was not performed in the previous study

Our study had several limitations. First, the effect of native x-ray attenuation of unenhanced liver parenchyma and iodine circulation during enhancement study in real patients were not considered in our liver phantom. The consequence was the significant discrepancy in CT attenuation value at 80 kVp scanning between the parenchyma of phantom and that of real patients (130 HU vs. 74 HU, respectively). However, the result of our phantom study is still valid because CNR was not determined by the absolute attenuation value, but by the difference between the parenchyma and the lesion, which was reliably reproduced in our experiment. Second, our study was retrospective and therefore, there may have been a selection bias, which is unavoidable in a retrospective study. However, we applied strict criteria for inclusion and exclusion. Third, a significant increase in lesion conspicuity, which was shown in our study by analyzing the CNR, FOM and qualitative study of the confirmed HCC lesions does not mean better diagnostic performance by itself. Better conspicuity of an arterial enhancing lesion might increase the false positive diagnosis for HCC due to the greater detection of arterioportal shunts or heterogeneous parenchymal enhancement. Therefore, further prospective clinical studies are warranted to prove the improvement in diagnostic performance such as evaluating the sensitivity and specificity by implementing the IRIS algorithm with a higher level of evidence. Fourth, there were several patients without histopathologic proof of their lesions. Fifth, the majority of patients enrolled in this study had relatively small to medium body habitus with a BMI smaller than 30. Thus, the conclusion of this study should be applied with caution to the patients with a BMI higher than 30. Last, IRIS reconstructed images failed to show a better overall image quality score, which was made on the subjective impression of the image by observers despite the lower noise and higher lesion conspicuity; this may be the result of the unfamiliarity of plastic-like image impressions of iterative reconstruction (26). The possibility that this unfamiliarity of the characteristic images generated by IRIS may negatively influence the interpretation of radiologists should be considered before the implementation of IRIS into routine clinical abdominal imaging.

In conclusion, the IRIS algorithm yields a significant improvement in image quality for MDCT images at low tube voltage (80 kVp), intermediate tube current (340 mAs) setting and further, may be effective for reducing patient radiation dose and for improving the conspicuity of hyperenhancing HCCs in thin adults when compared with standard 120 kVp CT images using the FBP reconstruction algorithm.

REFERENCES

1. Bruix J, Sherman M; American Association for the Study of Liver Diseases. Management of hepatocellular carcinoma: an update. *Hepatology* 2011;53:1020-1022. doi: 10.1002/hep.24199
2. Bruix J, Sherman M, Llovet JM, Beaugrand M, Lencioni R, Burroughs AK, et al. Clinical management of hepatocellular carcinoma. Conclusions of the Barcelona-2000 EASL conference. European Association for the Study of the Liver. *J Hepatol* 2001;35:421-430
3. Sherman M. The radiological diagnosis of hepatocellular carcinoma. *Am J Gastroenterol* 2010;105:610-612
4. Schindera ST, Nelson RC, Yoshizumi T, Toncheva G, Nguyen G, DeLong DM, et al. Effect of automatic tube current modulation on radiation dose and image quality for low tube voltage multidetector row CT angiography: phantom study. *Acad Radiol* 2009;16:997-1002
5. Funama Y, Awai K, Miyazaki O, Nakayama Y, Goto T, Omi Y, et al. Improvement of low-contrast detectability in low-dose hepatic multidetector computed tomography using a novel adaptive filter: evaluation with a computer-simulated liver including tumors. *Invest Radiol* 2006;41:1-7
6. Funama Y, Awai K, Nakayama Y, Kakei K, Nagasue N, Shimamura M, et al. Radiation dose reduction without degradation of low-contrast detectability at abdominal multisection CT with a low-tube voltage technique: phantom study. *Radiology* 2005;237:905-910
7. Leoni S, Piscaglia F, Golfieri R, Camaggi V, Vidili G, Pini P, et al. The impact of vascular and nonvascular findings on the noninvasive diagnosis of small hepatocellular carcinoma based on the EASL and AASLD criteria. *Am J Gastroenterol* 2010;105:599-609
8. Kim KW, Lee JM, Klotz E, Park HS, Lee DH, Kim JY, et al. Quantitative CT color mapping of the arterial enhancement fraction of the liver to detect hepatocellular carcinoma. *Radiology* 2009;250:425-434
9. Kim SH, Choi BI, Lee JY, Kim SJ, So YH, Eun HW, et al. Diagnostic accuracy of multi-/single-detector row CT and contrast-enhanced MRI in the detection of hepatocellular

carcinomas meeting the milan criteria before liver transplantation. *Intervirology* 2008;51 Suppl 1:52-60
10. McCollough CH, Primak AN, Braun N, Kofler J, Yu L, Christner J. Strategies for reducing radiation dose in CT. *Radiol Clin North Am* 2009;47:27-40
11. Lencioni R, Llovet JM. Modified RECIST (mRECIST) assessment for hepatocellular carcinoma. *Semin Liver Dis* 2010;30:52-60
12. Israel GM, Cicchiello L, Brink J, Huda W. Patient size and radiation exposure in thoracic, pelvic, and abdominal CT examinations performed with automatic exposure control. *AJR Am J Roentgenol* 2010;195:1342-1346
13. Guimarães LS, Fletcher JG, Harmsen WS, Yu L, Siddiki H, Melton Z, et al. Appropriate patient selection at abdominal dual-energy CT using 80 kV: relationship between patient size, image noise, and image quality. *Radiology* 2010;257:732-742
14. Kalra MK, Maher MM, Blake MA, Lucey BC, Karau K, Toth TL, et al. Detection and characterization of lesions on low-radiation-dose abdominal CT images postprocessed with noise reduction filters. *Radiology* 2004;232:791-797
15. Marin D, Nelson RC, Schindera ST, Richard S, Youngblood RS, Yoshizumi TT, et al. Low-tube-voltage, high-tube-current multidetector abdominal CT: improved image quality and decreased radiation dose with adaptive statistical iterative reconstruction algorithm--initial clinical experience. *Radiology* 2010;254:145-153
16. Marin D, Nelson RC, Samei E, Paulson EK, Ho LM, Boll DT, et al. Hypervascular liver tumors: low tube voltage, high tube current multidetector CT during late hepatic arterial phase for detection--initial clinical experience. *Radiology* 2009;251:771-779
17. Nakayama Y, Awai K, Funama Y, Hatemura M, Imuta M, Nakaura T, et al. Abdominal CT with low tube voltage: preliminary observations about radiation dose, contrast enhancement, image quality, and noise. *Radiology* 2005;237:945-951
18. Schindera ST, Nelson RC, Mukundan S Jr, Paulson EK, Jaffe TA, Miller CM, et al. Hypervascular liver tumors: low tube voltage, high tube current multi-detector row CT for enhanced detection--phantom study. *Radiology* 2008;246:125-132
19. Moon JH, Park EA, Lee W, Yin YH, Chung JW, Park JH, et al. The diagnostic accuracy, image quality and radiation dose of 64-slice dual-source CT in daily practice: a single institution's experience. *Korean J Radiol* 2011;12:308-318
20. Sigal-Cinqualbre AB, Hennequin R, Abada HT, Chen X, Paul JF. Low-kilovoltage multi-detector row chest CT in adults: feasibility and effect on image quality and iodine dose. *Radiology* 2004;231:169-174
21. Yeh BM, Shepherd JA, Wang ZJ, Teh HS, Hartman RP, Prevrhal S. Dual-energy and low-kVp CT in the abdomen. *AJR Am J Roentgenol* 2009;193:47-54
22. Nuyts J, De Man B, Dupont P, Defrise M, Suetens P, Mortelmans L. Iterative reconstruction for helical CT: a simulation study. *Phys Med Biol* 1998;43:729-737
23. Lasio GM, Whiting BR, Williamson JF. Statistical reconstruction for x-ray computed tomography using energy-integrating detectors. *Phys Med Biol* 2007;52:2247-2266
24. Gunn ML, Kohr JR. State of the art: technologies for computed tomography dose reduction. *Emerg Radiol* 2010;17:209-218
25. Kim YJ, Han JK, Kim SH, Jeong JY, An SK, Han CJ, et al. Small-bowel obstruction in a phantom model of ex vivo porcine intestine: comparison of PACS stack and tile modes for CT interpretation. *Radiology* 2005;236:867-871
26. Tipnis S, Ramachandra A, Huda W, Hardie A, Schoepf J, Costello P, et al. Iterative reconstruction in image space (IRIS) and lesion detection in abdominal CT. *Medical Imaging* 2010;7622:1-12
27. Pontana F, Pagniez J, Flohr T, Faivre JB, Duhamel A, Remy J, et al. Chest computed tomography using iterative reconstruction vs filtered back projection (Part 1): Evaluation of image noise reduction in 32 patients. *Eur Radiol* 2011;21:627-635
28. Samei E, Dobbins JT 3rd, Lo JY, Tornai MP. A framework for optimising the radiographic technique in digital X-ray imaging. *Radiat Prot Dosimetry* 2005;114:220-229
29. Kim KS, Lee JM, Kim SH, Kim KW, Kim SJ, Cho SH, et al. Image fusion in dual energy computed tomography for detection of hypervascular liver hepatocellular carcinoma: phantom and preliminary studies. *Invest Radiol* 2010;45:149-157
30. Prakash P, Kalra MK, Gilman MD, Shepard JA, Digumarthy SR. Is weight-based adjustment of automatic exposure control necessary for the reduction of chest CT radiation dose? *Korean J Radiol* 2010;11:46-53
31. Fletcher JG, Takahashi N, Hartman R, Guimaraes L, Huprich JE, Hough DM, et al. Dual-energy and dual-source CT: is there a role in the abdomen and pelvis? *Radiol Clin North Am* 2009;47:41-57
32. Fleischmann D, Kamaya A. Optimal vascular and parenchymal contrast enhancement: the current state of the art. *Radiol Clin North Am* 2009;47:13-26
33. Yoon SH, Lee JM, So YH, Hong SH, Kim SJ, Han JK, et al. Multiphasic MDCT enhancement pattern of hepatocellular carcinoma smaller than 3 cm in diameter: tumor size and cellular differentiation. *AJR Am J Roentgenol* 2009;193:W482-W489
34. McCollough CH, Bruesewitz MR, Kofler JM Jr. CT dose reduction and dose management tools: overview of available options. *Radiographics* 2006;26:503-512
35. Graser A, Johnson TR, Chandarana H, Macari M. Dual energy CT: preliminary observations and potential clinical applications in the abdomen. *Eur Radiol* 2009;19:13-23
36. 1990 Recommendations of the International Commission on Radiological Protection. *Ann ICRP* 1991;21:1-201
37. Rigby AS. Statistical methods in epidemiology. v. Towards an understanding of the kappa coefficient. *Disabil Rehabil* 2000;22:339-344
38. Szucs-Farkas Z, Kurmann L, Strautz T, Patak MA, Vock P, Schindera ST. Patient exposure and image quality of low-dose pulmonary computed tomography angiography: comparison of 100- and 80-kVp protocols. *Invest Radiol* 2008;43:871-876
39. Szucs-Farkas Z, Strautz T, Patak MA, Kurmann L, Vock P,

Schindera ST. Is body weight the most appropriate criterion to select patients eligible for low-dose pulmonary CT angiography? Analysis of objective and subjective image quality at 80 kVp in 100 patients. *Eur Radiol* 2009;19:1914-1922